



# Diagnosis of Liner Scuffing Fault of a Diesel Engine via Vibration and Acoustic Emission Analysis

Sangharatna M. Ramteke<sup>1</sup> · H. Chelladurai<sup>1</sup> · M. Amarnath<sup>2</sup>

Received: 7 August 2019 / Revised: 6 September 2019 / Accepted: 18 September 2019 / Published online: 3 October 2019  
© Krishtel eMaging Solutions Private Limited 2019

## Abstract

**Purpose** Cylinder liner, piston rings, and piston are the key components which contribute to the overall performance and efficiency of the IC engines. Excessive temperature and pressure inside the combustion chamber, abrasive wear on the surfaces of liner and piston are major factors which degrade the performance and efficiency of the IC engines. The abnormal function of IC engine components causes an increase in sound and vibration levels of the engine structure and degrades the overall performance. The purpose of this work is to use signal processing techniques to extract fault-related information from sound and vibration signals of the IC engine.

**Methods** This work considers Fast Fourier transform and statistical feature extraction methods for monitoring the liner scuffing fault developed in the diesel engine. The performance, emissions, and cylinder pressure were also monitored to analyze the effect of liner scuffing fault.

**Results and Conclusions** The results demonstrated that the aforementioned vibration signal analysis methods can be employed for the detection of liner scuffing fault in a diesel engine. The vibration and acoustic emission levels of the diesel engine were increased due to liner scuffing fault at all the loading conditions. The statistical feature parameters were increased at all the loading conditions due to the spurious effect of high-frequency amplitudes of vibration and acoustic signals. Furthermore, the performance parameters of the diesel engine were affected due to frictional losses caused due to liner scuffing fault.

**Keywords** Diesel engine · Liner scuffing fault · Fast Fourier transform · Exhaust emission

## List of Symbols

$a_x$	Vertical acceleration of the engine body ( $m/s^2$ )
$a_y$	Lateral acceleration of the engine body ( $m/s^2$ )
BDC	Bottom dead center
BP	Brake power (kW)
BTh	Brake thermal efficiency (%)
BSFC	Brake-specific fuel consumption ( $\frac{kg}{kWh}$ )
CO	Carbon monoxide (%)
CO <sub>2</sub>	Carbon dioxide (%)
DAQ	Data acquisition system

dB	Noise measured in decibel
FFT	Fast Fourier transform
FC	Fuel consumption ( $\frac{kg}{h}$ )
$F_x$	Vertical component of the inertia force (N)
$F_y$	Horizontal component of the inertia force (N)
HC	Hydrocarbon (ppm)
$k$	Frequency index (Hz)
$l$	Length of the connecting rod (mm)
$m_p$	Mass of piston (kg)
$m_c$	Mass of the crank (kg)
$m_{engine}$	Mass of the engine body (kg)
$n$	Time index (s)
$N$	Number of digitally acquired samples
NO <sub>x</sub>	Nitrogen oxide (ppm)
P	Piston
$p$	Measured sound pressure (Pa)
$p_{ref}$	Reference sound pressure (Pa)
$r$	Crank radius (mm)
SPL	Sound pressure level (dB)
TDC	Top dead center
$t$	Time period for revolution of crankshaft (s)

✉ M. Amarnath  
amarnath@iiitdmj.ac.in

<sup>1</sup> Internal Combustion Engine Laboratory, Department of Mechanical Engineering, Indian Institute of Information Technology Design and Manufacturing, Jabalpur 482005, India

<sup>2</sup> Tribology and Machine Dynamics Laboratory, Department of Mechanical Engineering, Indian Institute of Information Technology Design and Manufacturing, Jabalpur 482005, India

$\omega$	Angular velocity (rad/s)
$x_p$	Vertical displacement of piston (m)
$\dot{x}_p$	Velocity of piston in vertical direction (m/s)
$\ddot{x}_p$	Acceleration of piston in vertical direction (m/s <sup>2</sup> )
$x_c$	Vertical displacement of crankshaft (m)
$\dot{x}_c$	Velocity of crankshaft in vertical direction (m/s)
$\ddot{x}_c$	Acceleration of crankshaft in vertical direction (m/s <sup>2</sup> )
$x(k)$	Frequency domain signal
$x(n)$	Time-domain signal
$\bar{x}$	Mean value of the samples
$y_c$	Lateral displacement of piston (m)
$\dot{y}_c$	Velocity of crankshaft in lateral direction (m/s)
$\ddot{y}_c$	Acceleration of crankshaft in lateral direction (m/s <sup>2</sup> )
$\theta$	Angular displacement (rad)
$\sigma$	Standard deviation of the samples
$\lambda$	Wavelength (mm)
$\psi$	Angle between central axis and connecting rod (°)

## Introduction

Internal combustion engines (ICE) are the main source of power generation and have wide applications in the field of automobile, aerospace manufacturing, marine industry, etc., [1]. The main issues with the ICE are the performance and efficiency which depend on the performance of the cylinder liner, piston, and piston rings. These components are subjected to operate under high temperature and pressure inside the combustion chamber. The cylinder liner is subjected to various types of wear such as thermal cracks, cavitation on the inner walls, irregular surface wear, bright spots on the sliding surface area, etc. Therefore, it is of great importance to consider a condition-monitoring method which diagnoses the health of ICE components, thereby avoiding the unexpected shutdown of the system.

The condition monitoring of diesel engines has become one of the great areas of research among various researchers for decades. Most of the monitoring techniques are used to analyze the combustion phenomenon, which detects emissions of diesel engine such as carbon monoxide, hydrocarbon, nitrogen oxide, etc. Vibration and sound analysis are one of such condition-monitoring techniques which have attracted the researchers attention in fault diagnosis of the machine components. These techniques offer great potential to monitor the health of machine components due to their non-intrusive nature of the measurement and also provide dynamic and invisible information of the machine.

An increase in engine vibration and generation of abnormal noise are the indication of the failure of the main components such as cylinder liner, piston rings, and piston of the

diesel engine. Acquisition of vibration and sound signals of the engine in healthy condition and comparing these signals with the signals acquired under the faulty condition is the main approach of this analysis. Every mechanical system has unique frequency characteristics associated with the health of components. The diesel engine has some frequency characteristics related to its components. When the fault occurs in the diesel engine, these frequency characteristic increase significantly. Variations in frequency components can be recorded using some signal processing techniques such as fast Fourier transform (FFT), short-time Fourier transforms (STFT), and continuous wavelet transforms (CWT) etc. These spectral features can be attributed to a specific fault [2].

Moosavian et al. [3] investigated the effect of piston scuffing fault on the performance of spark ignition (SI) engine. The authors analyzed engine vibration signals using CWT technique. The statistical parameters of the vibration signals such as maximum, mean, root mean square (RMS), skewness, kurtosis, and crest factor were considered to obtain the effect of piston scuffing fault on the engine vibration. The results revealed that piston scuffing fault was significantly affected engine vibrations and performance. Moosavian et al. [4] carried out experiments to analyze the effect of piston scratching fault on the vibration behaviour of the SI engine. By considering STFT and CWT methods for vibration analysis, the authors have concluded that the piston scratching fault results in a significant increase in the engine vibration levels. The statistical parameters of vibration signals were considered to highlight the piston scratching fault. Chiatti et al. [5] conducted an experimental study to investigate the vibro-acoustic behaviour of a city-car engine fueled with blends of distilled biodiesel. The results revealed that the RMS values of the acceleration signal were significantly affected by all the tested blends. These values showed an increase in trend with respect to increase in engine speed. Authors have correlated the frequency components obtained from noise radiations to the combustion process. Gutierrez et al. [6] studied the engine vibrations based on the fuel blends obtained from recycled lubricating oil and diesel fuel. For analyzing the vibration behaviour, the FFT method was employed. The results revealed that engine vibration was significantly reduced for the fuel blends as compared to neat diesel fuel. The fuel properties such as flash point, cetane number, and the heat value played an important role in minimizing the engine vibrations and improving the performance of the engine. Barelli et al. [7] proposed a new diagnosis methodology for ICE based on vibration and acoustic pressure measurements. The vibration and acoustic signals were acquired from the engine head to indicate the combustion phenomenon. The results showed that vibration and acoustic pressure signals were greatly influenced by the combustion pressure and frequency components. Celebi et al. [8]

carried out experimental investigations to analyze the effect of blends of high viscosity biodiesel fuel and hydrogen on the fuel consumption and vibration behaviour of compression ignition (CI) engine. Authors have used the biodiesel which was obtained from the *Pongamia pinnata* and Tung oil. Blends were prepared with the low sulphur diesel fuel and hydrogen gas was allowed through the intake manifold to analyze the combined effect with high viscous biodiesel fuels. The results revealed a comparatively minimum specific fuel consumption of these blends due to the addition of hydrogen. The vibration acceleration of the engine was found less in both biodiesel and hydrogen blends. Erinc et al. [9] conducted experimental investigations to analyze the effect of biodiesel blends obtained from sunflower, canola, and corn with hydrogen on the vibration, noise, and exhaust emissions of CI engine. Results highlighted the importance of the addition of hydrogen in biodiesel blends to reduce engine vibration levels. Sound pressure level lessening with diesel–biodiesel blend as compared to neat diesel, and authors have concluded that the exhaust emissions such as  $\text{CO}_2$  and  $\text{NO}_x$  were increased significantly with the usage of biodiesel blends and CO emission was found to be decreased with biodiesel blends and hydrogen. Taghizadeh et al. [10] studied the combustion and vibration behaviour of a diesel engine using biodiesel blends. Authors stated that STFT and Morlet scalogram (MSC) methods were able to detect the faults and knocks in an engine caused due to the combustion of diesel fuels and biodiesel blends. It was also proposed that MSC is a suitable method for detecting faults in the fuel injection system. Kerimcan et al. [11] carried out experimental investigations to evaluate the effect of biodiesel blends obtained from the sunflower and canola with the addition of natural gas on the vibration and sound signal characteristics of the diesel engine. The experimental outcomes revealed that the vibration and sound pressure level were decreased with the application of biodiesel blends as compared to neat diesel fuel. The authors also postulated that the addition of natural gas helped to reduce these parameters even more. Uludamar et al. [12] conducted an experimental study to examine the effect of biodiesel blends on the noise and vibration of the CI engine. Authors used a linear and non-linear regression analysis to establish the relationship between noise vibration and fuel properties of the biodiesel blends. The experimental outcomes revealed that the vibration and noise of the CI engine decreased with the increasing biodiesel ratio. Ahmad et al. [13] studied the vibration behaviour of the diesel engine using biodiesel and petrodiesel fuel blends. Authors have used biodiesel which was produced from vegetable oils such as canola and soybeans, animal fats, and waste oil. By considering nine different fuel blends named as B5, B10, B15, B20, B30, B40, B50, neat biodiesel (B100), and neat petrodiesel (D100), the results revealed that the vibration of the engine varied

significantly with the fuel blends. Lower vibration levels were obtained for B40 and B20 fuel blends due to least fluctuation of cylinder pressure. However, engine vibration was lower for D100 as compared to B100. The highest values of engine vibration were obtained for B15, B30, and B50 biodiesel blends due to fuel cetane number and injection advance.

Ahmad et al. [14] carried out experimental investigations to analyze the effect of added ethanol to diesel fuel for monitoring performance, vibration, combustion, and knocking of CI engine. The ethanol was added to diesel fuel in the concentration of 2, 4, 6, 8, 10, and 12%. The results showed that an increase in ethanol content more than 8% in the diesel fuel caused longer ignition delay and decreased the performance of the engine. However, the longer ignition delay caused a change in pressure inside the combustion chamber and initiated the knocking phenomenon. The authors also reported that the variation in RMS values of vibration signals was observed due to pressure variation and inertia forces; however, the kurtosis values of vibration signal were due to the variation of pressure in the combustion chamber only. Jena and Panigrahi [15] established a process to identify the piston-bore defect by studying the noise of the engine using the CWT technique. The results revealed that the piston-bore defect modifies the engine noise considerably in the lower frequency range. Authors suggested that the complex morlet wavelet was appropriate to detect the piston-bore defect as compared to CWT bi-orthogonal wavelet. Giancarlo et al. [16] carried out an experimental investigation to study the in-cylinder pressure generation during the combustion process using acoustic emission analysis. The relationship between the injection and combustion process was correlated to engine noise radiation.

The aforementioned literature survey showed that most of the research works were carried out to analyze the effect of biodiesel blends on the vibration and acoustic emission analysis of diesel engines. Some research articles showed the application of signal processing techniques, viz., FFT and CWT, to analyze the vibration and acoustic emission signals. However, very few research works have considered signal processing tools to diagnose faults developed on engine components. Therefore, in the present research work, an attempt has been made to diagnose the cylinder liner scuffing fault using vibration and acoustic emission analysis by considering FFT and statistical feature analyses. To detect the cylinder liner scuffing fault, engine performance and emission parameters were also considered in the current study.

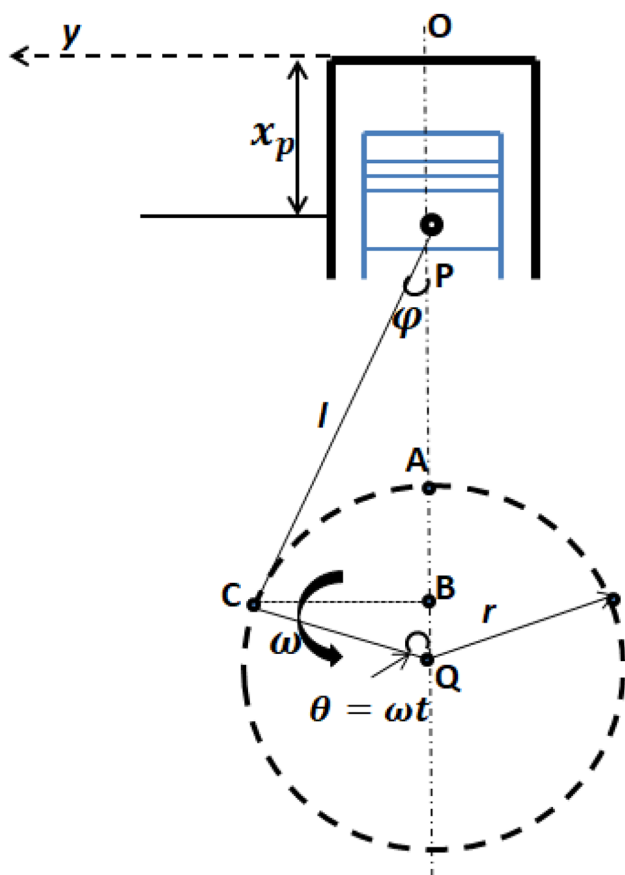


**Fig. 1** The schematic view showing the motion of piston, connecting rod, and crank [14]

## Concepts of Engine Vibration, Acoustic Emission, and Analysis Methods

### Displacement, Velocity, and Acceleration of the Piston

The vibrations of the diesel engine are mainly due to three sources. The primary source of engine vibration is the upward and downward motion of a piston in the cylinder liner. The secondary source of engine vibration is the conversion of linear motion to rotational motion of crankshaft/crank. The tertiary source of engine vibration occurs due to the rate of pressure rise in the combustion chamber which exerts unequal stresses on the piston crown. The inertia forces generated by the motion of the piston, connecting rod and crank result in engine vibrations [12, 13]. Figure 1 depicts the schematic view of the reciprocating engine having piston ( $P$ ), connecting rod ( $l$ ), and crank of the radius ( $r$ ). The crankshaft rotates in an anti-clockwise direction with angular velocity  $\omega$ . Point  $O$  is designated as the origin of the central axis  $x$  up to which the piston attains its maximum position. The displacement of the piston  $P$  inside the cylinder liner with an angular displacement

of  $\theta = \omega t$  is shown in Fig. 1. The vertical displacement, velocity, and acceleration of the piston  $P$  can be expressed as given in Eqs. (1–3), respectively.

$$x_p = r \left( 1 + \frac{r}{2l} \right) - r \left( \cos \omega t + \frac{r}{2l} \cos^2 \omega t \right) \quad (1)$$

$$\dot{x}_p = r\omega \left( \sin \omega t + \frac{r}{2l} \sin 2\omega t \right) \quad (2)$$

$$\ddot{x}_p = r\omega^2 \left( \cos \omega t + \frac{r}{l} \cos 2\omega t \right). \quad (3)$$

### Displacement, Velocity, and Acceleration of the Crank/Crankshaft

The vertical and horizontal displacement, velocity, and acceleration of the crank/crankshaft with respect to  $XY$  coordinate axis are given in Eqs. (4–9):

$$x_c = l + r(1 - \cos \omega t) \quad (4)$$

$$y_c = r \sin \omega t \quad (5)$$

$$\dot{x}_c = r\omega \sin \omega t \quad (6)$$

$$\dot{y}_c = r\omega \cos \omega t \quad (7)$$

$$\ddot{x}_c = r\omega^2 \cos \omega t \quad (8)$$

$$\ddot{y}_c = -r\omega^2 \sin \omega t. \quad (9)$$

### Inertia Forces Generated by Piston and Crankshaft/Crank

For calculating the vertical and horizontal components of the inertia forces, lumped mass analysis is considered in which the mass of the connecting rod is concentrated at two ends such as piston end and crank-pin end, and  $m_p$  and  $m_c$  denote the mass of the piston and mass of the crank pin, respectively. The vertical and horizontal components of the inertia forces  $F_x$  and  $F_y$  can be expressed by Eqs. (10) and (11):

$$F_x = (m_p + m_c)r\omega^2 \cos \omega t + m_p \frac{r^2\omega^2}{l} \cos 2\omega t \quad (10)$$

$$F_y = -m_c r\omega^2 \sin \omega t, \quad (11)$$

where  $F_x$  and  $F_y$  are the vertical and horizontal components of the inertia forces, and  $m_p$  and  $m_c$  denote the mass of the piston and crank, respectively.

Furthermore, it is observed that the acceleration of the piston and crankshaft/crank is directly proportional to the engine angular velocity  $\omega$ . If  $m_{\text{engine}}$  be the mass of the engine body, the vertical ( $a_x$ ) and lateral ( $a_y$ ) acceleration of the engine body



can be expressed as given in Eqs. (12) and (13), respectively [14]:

$$a_x = \frac{(m_p + m_c)r\omega^2 \cos \omega t + m_p \frac{r^2\omega^2}{l} \cos 2\omega t}{m_{\text{engine}} - m_p - m_c} \tag{12}$$

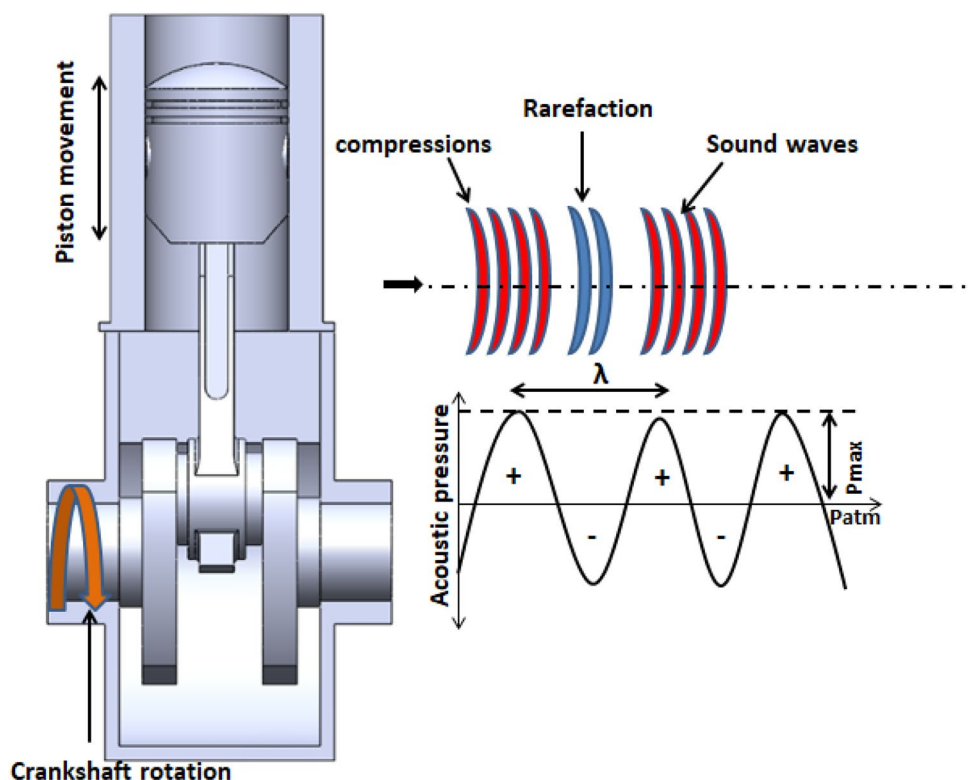
$$a_y = \frac{-m_c r \omega^2 \sin \omega t}{m_{\text{engine}} - m_c} \tag{13}$$

### Acoustic Emission of Engine

Acoustic emission from the diesel engine occurs due to excitation forces caused by the movement of reciprocating and rotating components such as piston, connecting rods, and crankshaft. The other auxiliary equipment, viz., intake and exhaust valve, valve train, fuel injector, gears, etc., which causes the engine to vibrate [17]. The vibration of the engine block due to the movement of these components emits noise radiation. On the other hand, the main source of engine acoustic emission is the combustion phenomenon occurring in engine. The forces during combustion generate acoustic frequencies in the range of 500–5000 Hz [18]. The overall noise emitted from the engine is calculated by adding all these excitation forces which is given in Eq. (14):

$$\text{dB}_{\text{Overall}} = \text{dB}_{\text{Combustion}} + \text{dB}_{\text{Piston slap}} + \text{dB}_{\text{Injection}} + \text{dB}_{\text{Valvetrains}} + \text{dB}_{\text{Gears}} + \text{dB}_{\text{Other accessories}} \tag{14}$$

**Fig. 2** The schematic view showing the representation of the sound waves produced by the engine [17]



Noise emitted from the engine is the fluctuation of sound pressure about the ambient atmospheric pressure in an elastic medium such as air, water, and solids, generated by the vibrating body. This noise propagates in the longitudinal direction involving the compression and rarefaction in any one of the media (air in this case), as shown in Fig. 2. Wavelength λ is the distance between the successive compression and rarefaction which is also the distance travelled by the sound wave during one cycle. The sound pressure level in the diesel engine at any point is given by Eq. (15) [18]:

$$\text{SPL} = 20 \log_{10} \left( \frac{p}{p_{\text{ref}}} \right), \tag{15}$$

where SPL is sound pressure level (dB), *p* is measured sound pressure (Pa), and *p<sub>ref</sub>* is reference sound pressure which is  $2 \times 10^{-5}$  Pa.

### Fast Fourier Transform

In many mechanical systems, the frequency of occurrence is generally associated with the health of systems. Often, time-domain signals do not provide useful information, while on the other hand, frequency domain signals provide some useful frequency ranges associated with the machinery. To extract the useful information from the time-domain signals, it is essential to transform the signals into the frequency domain. Therefore, to analyze the vibration and acoustic signals, the FFT method

was employed. For a digital set of time-domain data  $x(n)$ , the FFT can be computed by Eq. (16) [14]:

$$x(k) = \sum_{n=0}^{N-1} x(n) \cdot e^{-\frac{2\pi n k j}{N}}, \quad (16)$$

where  $n$  and  $k$  are the time and frequency index.  $N$  is the number of sampled data.

Furthermore, statistical features were also extracted to analyze the vibration and acoustic signals. The most commonly used parameters are mean, standard deviation, skewness, and kurtosis [3]. A brief explanation about the used parameters is given below.

### Mean

The mean value of the vibration and acoustic signals in the time domain can be computed by Eq. (17):

$$\bar{x} = \frac{1}{N} \sum_{i=1}^N x_i. \quad (17)$$

### Standard Deviation

The effective power or energy content of the signal can be obtained by computing standard deviation of those signals. The standard deviation  $\sigma$  of the signal can be calculated using Eq. (18):

$$\sigma = \sqrt{\frac{1}{N} \sum_{i=1}^N (x_i - \bar{x})^2}. \quad (18)$$

### Skewness

The skewness of the signals describes the asymmetry in the statistical distribution of data about its mean value and it can be calculated using Eq. (19):

$$x_{\text{Skewness}} = \frac{\sum_{i=1}^N (x_i - \bar{x})^3}{(N-1)\sigma^3}. \quad (19)$$

### Kurtosis

Kurtosis describes the sharpness of the signals. The kurtosis value can be obtained by Eq. (20):

$$x_{\text{Kurtosis}} = \frac{\sum_{i=1}^N (x_i - \bar{x})^4}{(N-1)\sigma^4}. \quad (20)$$

Monitoring the performance of the engine is one of the criteria to diagnose the fault. The propagation of faults in engine results in a reduction in the performance parameters such as brake power and brake thermal efficiency and increase in brake-specific fuel consumption and fuel consumption. The performance parameters monitored in this analysis are calculated by Eqs. (21–23).

### Brake Power

The brake power is the total power output of the engine. It can be calculated by Eq. (21):

$$BP = \frac{2\pi NT}{60,000}, \quad (21)$$

where BP is the brake power (kW),  $N$  is the engine speed in rpm, and  $T$  is the engine torque (N m).

### Brake Thermal Efficiency

The overall efficiency of the engine is known as brake thermal efficiency. It is given by Eq. (22):

$$BTh(\%) = \frac{BP \text{ (kW)} \times 3600}{\text{Fuel flow} \left(\frac{\text{kg}}{\text{h}}\right)} \times \text{Calorific value} \left(\frac{\text{kJ}}{\text{kg}}\right). \quad (22)$$

### Brake-Specific Fuel Consumption

The amount of fuel required to produce brake power of the engine is known as brake-specific fuel consumption (BSFC) which can be calculated by Eq. (23):

$$BSFC = \frac{\text{Fuel flow} \left(\frac{\text{kg}}{\text{h}}\right)}{BP \text{ (kW)}}. \quad (23)$$

### Fuel Consumption

Fuel consumption is the rate at which engine consumes fuel to produce the required power. It is measured in kg/h.

## Experimental Setup, Sensors, and Data Acquisition Procedure

In the present work, a single cylinder four-stroke diesel engine is employed to conduct the experiments. The setup is provided with the water-cooled eddy current dynamometer for loading arrangements which is having a loading range of 0–12 kg. A control panel is used to control the speed and load of the engine. The variations in load and speed are observed by an indicator provided by the control panel.

**Fig. 3** The actual experimental setup and its schematic

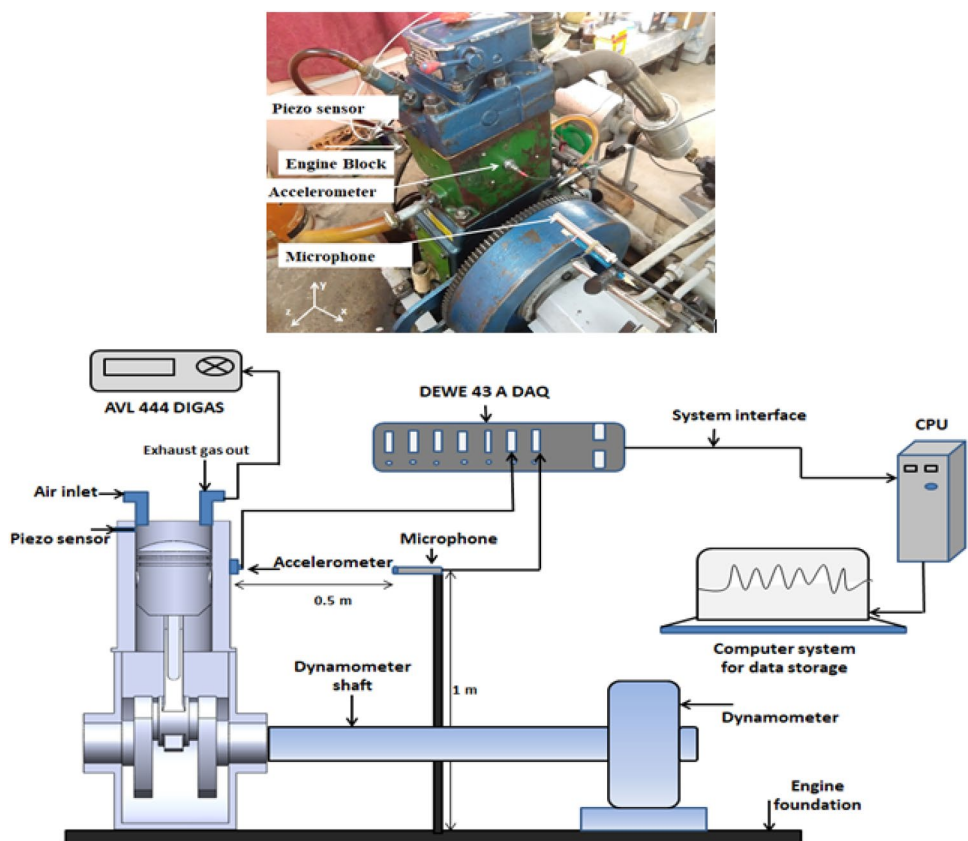


**Table 1** Specification of diesel engine

Engine	Kirloskar water cooled
Compression ratio	12–18:1
Rated power	3.5 kW @ 1500 RPM
Fuel	H.S diesel
Cylinder diameter	85 mm
No. of cylinder	1
No. of strokes	4
Stroke length	110 mm

National Instruments USB 6210 data acquisition system is used to monitor the performance of the engine. A piezoelectric pressure sensor is mounted on engine head to measure the combustion pressure. The specifications of the diesel

engine are given in Table 1, and the actual and schematic experimental setup is shown in Fig. 3. The engine performance is monitored using LabView based “EnginesoftLV” software.

A KS78.100 Piezoelectric uni-axial accelerometer manufactured by IDS Innomic GmbH is used to measure the vibration signals. The accelerometer is placed at three different locations on the engine block to measure the vibration in longitudinal (x), lateral (z), and vertical (y) axes. A 20 kHz sampling frequency used to acquire vibration signals. An MP201 ICP microphone manufactured by BSWA Technology Co., Ltd. is used to measure the acoustic signals from the engine. The microphone is placed 0.5 m away from the engine and 1 m above the ground surface. The sound signals are acquired in the near-field condition. The acoustic signals are sampled at 40 kHz sampling frequency; this frequency range is sufficient to disclose the frequency contents of acoustic signals. The vibration and

**Table 2** AVL 444 DIGAS exhaust gas analyzer specifications

Parameters	Measuring range	Accuracy
Carbon monoxide	0–10% vol	≤ 0.6% vol: ± 0.03% vol ≥ 0.6% vol: ± 5% vol
Carbon dioxide	0–20% vol	≤ 10% vol: ± 0.5% vol ≥ 10% vol: ± 5% vol
Hydro carbon	0–20,000 ppm	≤ 200 ppm: ± 10 ppm ≥ 200 ppm: ± 5% of ind.value
Nitrogen oxide	0–5000 ppm	≤ 500 ppm: ± 50 ppm

acoustic signals were passed through the DEWE-43A USB data acquisition system (DAQ) and recorded in a personal computer system through Dewesoft 7 software.

The exhaust emissions of diesel engine are measured using AVL 444 DIGAS exhaust gas analyzer whose specification is given in Table 2.

### Experimental Procedure

The diesel engine was operated for 10 h to satisfy the running in wear condition after the installation of a healthy liner, piston, and piston rings. The lubricating oil was changed after the running in wear period. Furthermore, the above-mentioned engine components were considered to conduct the experiments. The experiments were conducted in two stages as discussed below.

In the first stage of experiments, the vibration and sound signals were recorded under healthy operating condition of the engine. Figure 4 shows the pictorial view of healthy liner and piston, the dimension of the healthy liner measured with bore gauge is given in Table 3. The vibration and acoustic signals were acquired from the engine under healthy and faulty conditions, and the statistical parameters were extracted from the sound and vibration signals to detect the severity of faulty liner of the engine. The performance characteristics and exhaust emissions of diesel engine were also measured simultaneously.

In the second stage of experiments, the healthy liner was replaced with the faulty liner in the engine keeping the piston and piston rings in the healthy condition. The pictorial view of the faulty liner with scuffing marks on its inner surface is shown in Fig. 5a. It can be observed that the faulty

**Fig. 4** The pictorial view of healthy liner and piston

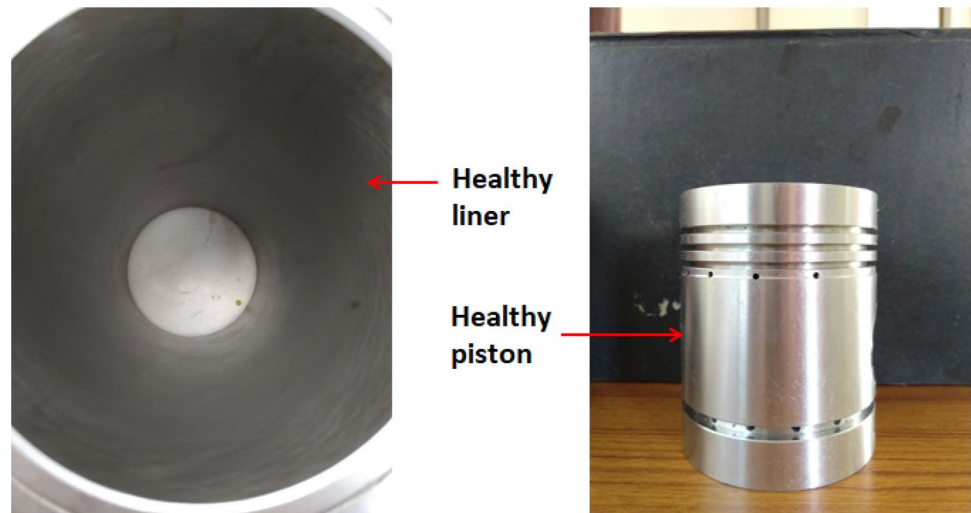


**Fig. 5** The pictorial view of a faulty liner with scuffing marks. **a** Thickness of the wear grooves

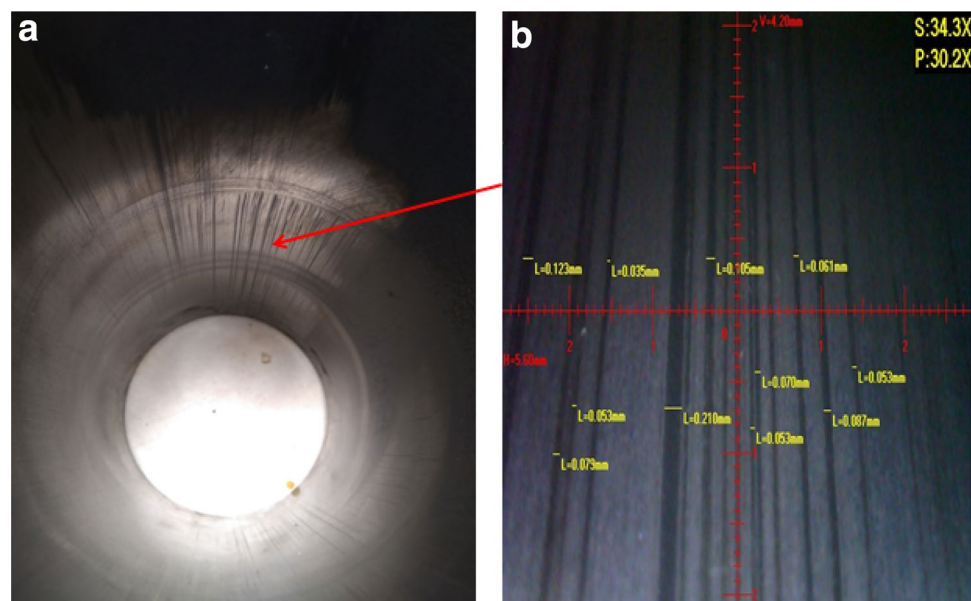




**Fig. 6** Flowchart showing the procedure for signal acquisition and analysis

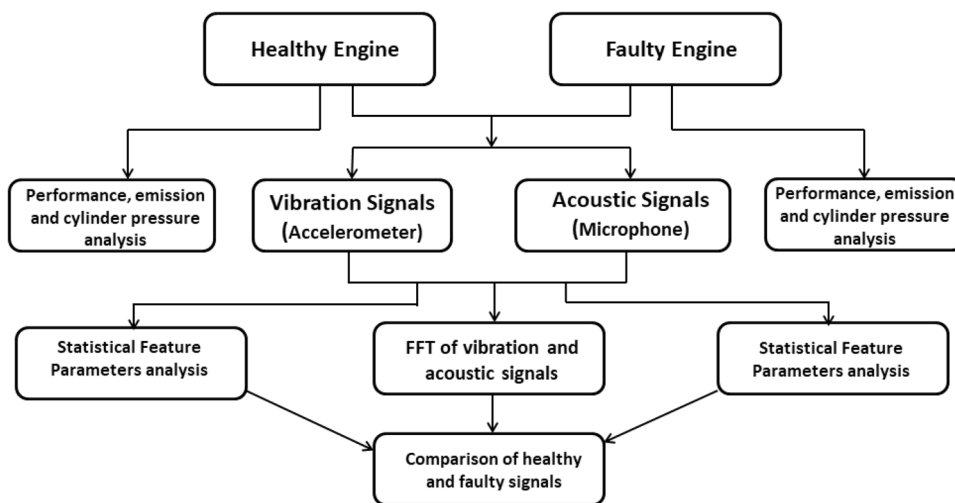


**Table 3** Dimension of the healthy and faulty liner

Parameters	Healthy liner (mm)	Faulty liner (mm)	Faulty liner with wear grooves (mm)
Top dead center (TDC)	85.02	85.29	85.98
Middle	85.02	85.92	85.96
Bottom dead center (BDC)	85.02	85.93	85.965

liner has severe wear grooves, i.e., scuffing on the inner wall which generally affects the engine vibration, acoustics, performance, and emissions. The depth and thickness of liner scuffing were measured with a bore gauge and USB microscope which is shown in Fig. 5b and Table 3, respectively. This condition of the engine was termed as faulty. The vibration and acoustic signals were measured under faulty condition of the liner. The statistical parameters were calculated to detect faulty engine conditions. The performance and emission parameters were also measured in conjunction with acoustic and vibration signals. The flowchart showing the procedure for signal acquisition and analysis is shown in Fig. 6.

## Results and Discussion

### Engine Vibration and Acoustic Analysis Using FFT

The vibration and acoustic signals were measured for both healthy and faulty engine conditions at various loads, viz., 0, 3, 6, 9, and 12 kg. The vibration signals were acquired in three different axes, namely, longitudinal (*x*), lateral (*z*), and vertical (*y*). The vibration and acoustic signals for healthy and faulty engine condition in the time domain are shown in Figs. 7 and 8, respectively. It was clearly observed that the liner scuffing fault substantially increased the vibration

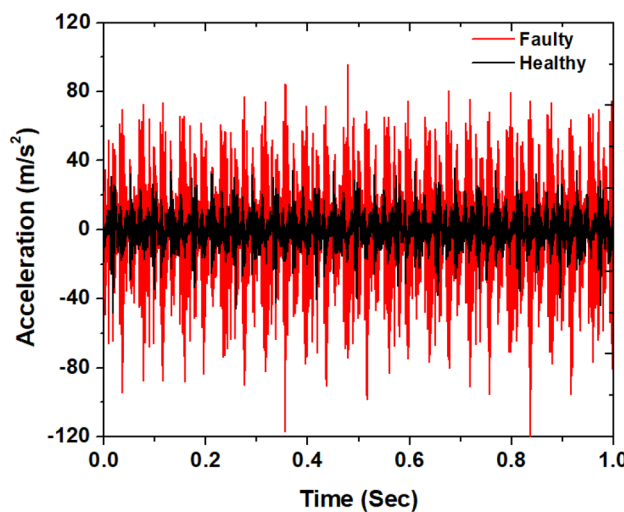


**Fig. 7** Vibration signals for healthy and faulty engine operating conditions in time domain

and acoustic signal amplitudes. This implied that the liner scuffing fault affected overall engine vibrations and acoustic emissions.

To analyze the effect of liner scuffing fault in detail, the time-domain vibration signals in all three axes were transformed to the frequency domain using FFT which is shown in Figs. 9, 10, and 11. It was observed from Fig. 9f–j that

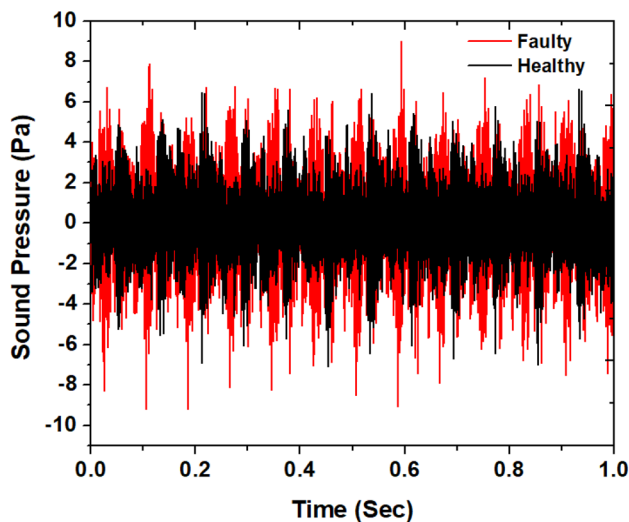


**Fig. 8** Acoustic signals for healthy and faulty engine operating conditions in time domain

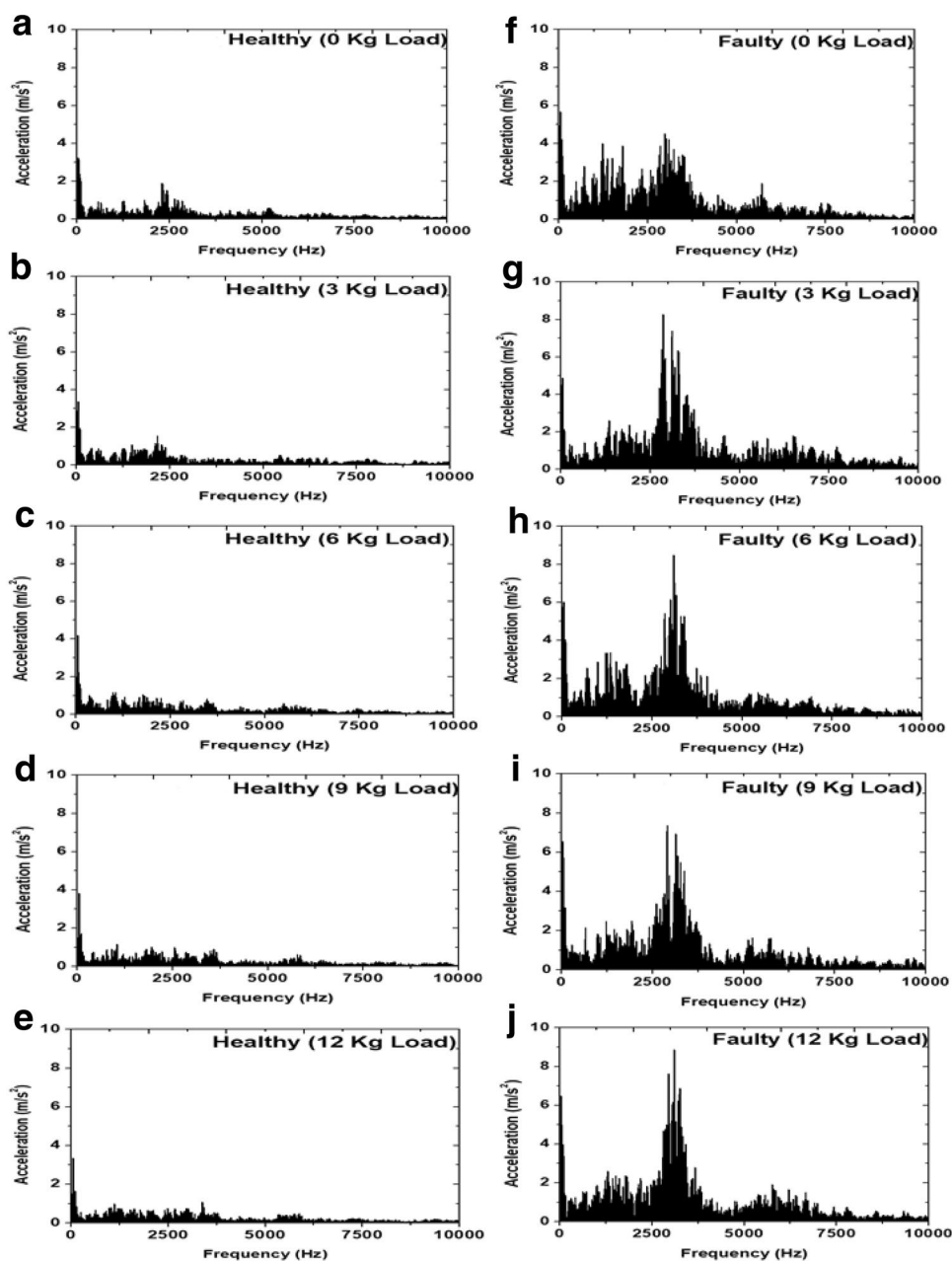
due to liner scuffing fault, excited frequency bands with higher amplitudes were perceived in all the loading conditions. The dominating frequency components of the vibrations acquired in the longitudinal ( $x$ ) axis were ranged from 0.5 to 4 kHz. The dominating frequency at which engine vibrates with higher amplitude was observed at 3.4 kHz. The higher amplitudes of vibrations were perceived at 3, 6, and 12 kg loads in longitudinal axes which are shown in Fig. 9g, h, j, respectively. At 12 kg load, engine vibrates with a maximum amplitude of  $9 \text{ m/s}^2$ , as shown in Fig. 9j. The longitudinal axis vibrations are generally due to the conversion of reciprocating motion of the piston to the rotational motion of crankshaft and inertia forces generated due to this motion. The FFT spectra of engine vibrations in the lateral ( $z$ ) axis shown in Fig. 10a–j indicated that the liner scuffing fault excited the frequency band of higher amplitudes in the range of 0.2–4.5 kHz. The dominating frequency component in the lateral axis was perceived at 2 kHz. The higher values of amplitude vibrations were perceived at 3 and 12 kg loads, whereas, at 12 kg load, the engine was having a higher amplitude of vibration, i.e.,  $8.2 \text{ m/s}^2$ , as shown in Fig. 10j. The vibrations in the lateral ( $z$ ) axis are generally due to the upward and downward motion of a piston in the cylinder liner. The vibration of the engine block in vertical ( $y$ ) axis is shown in Fig. 11a–j. It was observed that the liner scuffing faults excited the frequency band of higher amplitudes within the range of 0.2–2 kHz. The dominating frequency components in vertical axes were perceived in the range of 0.9–1.3 kHz. The vibrations in the vertical axes are generally due to combustion phenomenon in which the rate of pressure rise in the combustion chamber fluctuates continuously, which causes the engine to vibrate, especially engine head. The uneven pressure acting on the piston crown leads to

piston slap phenomenon which is also responsible for engine vibrations. The maximum vibration amplitudes were perceived at 3, 9, and 12 kg loads, which are shown in Fig. 11g, i, j, respectively. The maximum amplitude of vibration, i.e.,  $6.35 \text{ m/s}^2$ , was perceived at 9 kg load, which is shown in Fig. 11i. From the discussions, it can be interpreted that the liner scuffing fault significantly affected mechanical actions of the piston, connecting rod and crankshaft in longitudinal ( $x$ ) and lateral ( $z$ ) and vertical ( $y$ ) axes which caused maximum engine vibrations.

The FFT spectra of acoustic signals measured for both healthy and faulty engine conditions are presented in Fig. 12a–j, respectively. It was observed that amplitudes of sound pressure signals were increased significantly at all loading conditions. The maximum sound pressure amplitudes were perceived at all loads under faulty operating condition, as shown in Fig. 12f–j, which can be attributed to the liner scuffing fault in the engine cylinder. The acoustic emissions from the engine are observed mainly due to mechanical and combustion excitation. Liner scuffing fault strongly deteriorates the mechanical actions of ICE components such as piston, piston rings, connecting rod, crankshaft, etc. The combustion phenomenon gets affected by the liner scuffing fault which caused abnormal combustion in the combustion chamber, thereby causing engine noise radiation. The rubbing action of the piston–cylinder assembly might be another reason for increase in overall engine vibrations and noise levels [3].

Furthermore, the most commonly used statistical parameters such as mean, standard deviation, skewness, and kurtosis were extracted from the engine vibration and acoustic signals. These features were used to quantify the difference between healthy and faulty engine conditions. The statistical features of the vibration signals in all the three axes are presented in Figs. 13, 14, and 15. It was clearly observed that the mean and standard deviation values were increased substantially for all the loading conditions. This indicated that the energy content in the vibration signals was increased due to liner scuffing fault. The skewness of the vibration signals indicated that the data were asymmetrically distributed about its mean value due to liner scuffing fault. The kurtosis of the signals indicated that due to liner scuffing fault, the sharpness of vibration signals increased significantly. The uneven trend of all the statistical feature parameters was due to the spurious effect of high-frequency amplitude of vibrations in healthy and faulty operating conditions. In longitudinal ( $x$ ) axis, the maximum value of the mean, standard deviation, skewness, and kurtosis was perceived at 3, 6, 0, and 6 kg load, as shown in Fig. 13a–d, respectively. In lateral ( $z$ ) axis, the maximum values of the mean, standard deviation, skewness, and kurtosis were perceived at 6, 9, 9, and 0 kg loads, as shown in Fig. 14a–d, respectively. In vertical ( $y$ ) axis, the maximum values of the mean, standard deviation,

**Fig. 9** FFT spectra of engine vibrations in longitudinal ( $x$ ) axis: **a–e** healthy and load condition. **f–j** Faulty and load condition



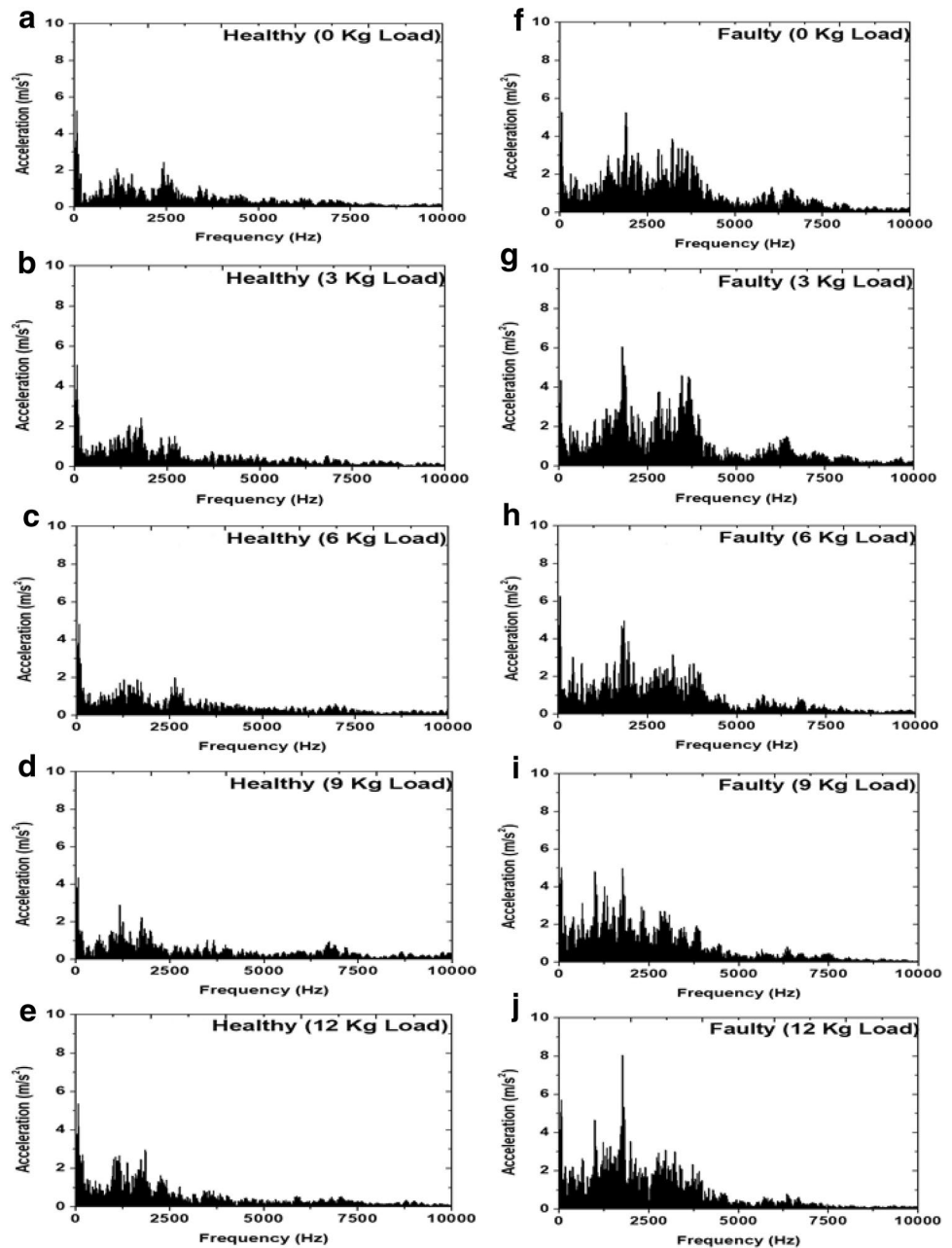
skewness, and kurtosis were perceived at 6, 12, 12, and 3 kg loads, as shown in Fig. 15a–d, respectively.

Furthermore, the statistical feature parameters were extracted for the engine acoustic signals which is shown in Fig. 16a–d. It was clearly observed that liner scuffing fault significantly increased the mean, standard deviation, skewness, and kurtosis values of the acoustic signals at all loading conditions. The maximum value of the mean, standard deviation, skewness, and kurtosis were perceived at 3, 12, 12, and 12 kg load, as shown in Fig. 15a–d, respectively.

## Performance, Emission, and Cylinder Pressure Analysis

The performance, emissions, and cylinder pressure were measured for both healthy and faulty engine conditions, which are shown in Figs. 17, 18, and 19, respectively. The most important performance parameters such as brake power (BP), brake thermal efficiency (BTh), brake-specific fuel consumption (BSFC), and fuel consumption (FC) were measured at distinct loading conditions and depicted in Fig. 17a–d. It was observed that the liner scuffing fault severely affected the engine performance. The decrement in BP and BTh was observed about 4.10% and

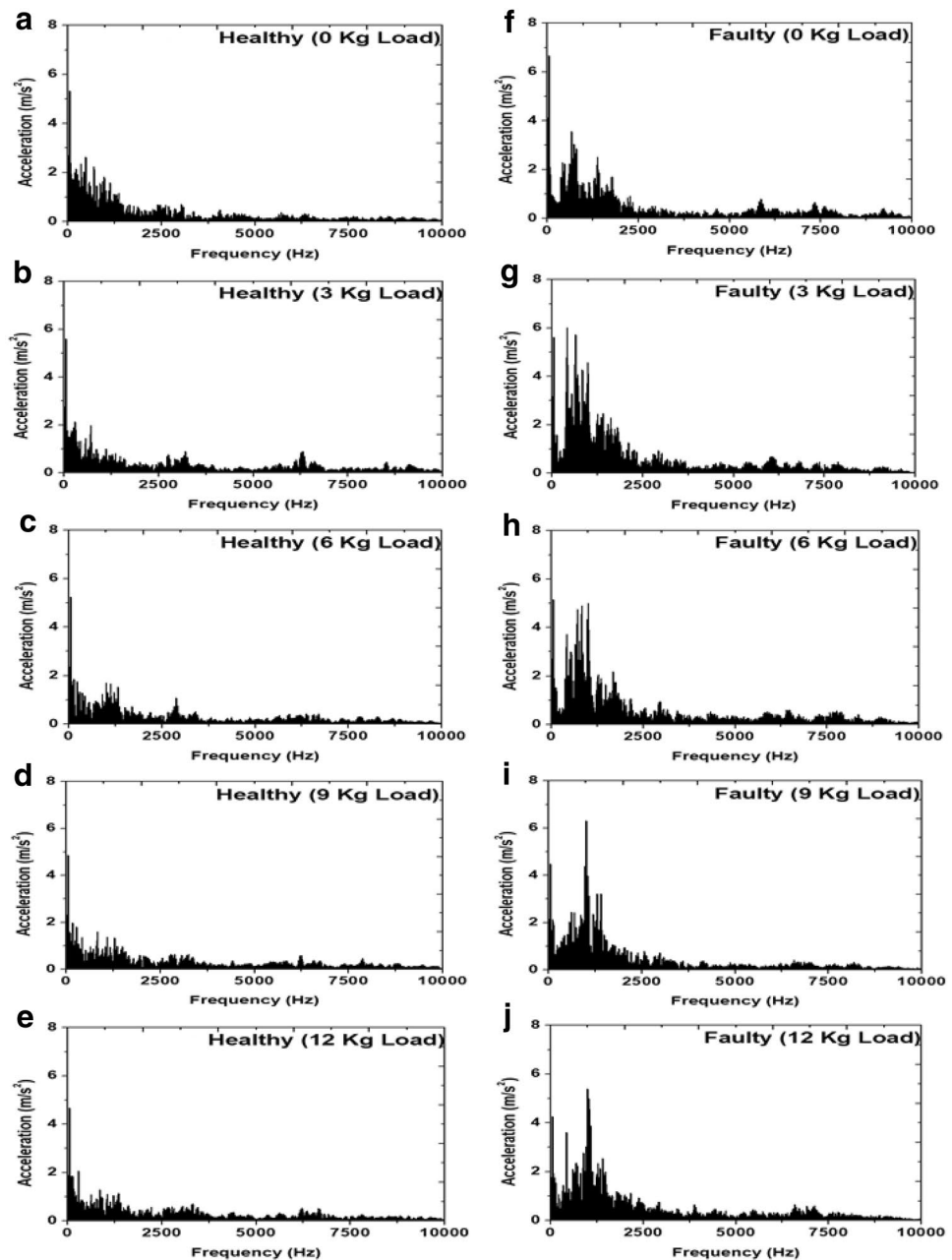
**Fig. 10** FFT spectra of engine vibrations in lateral ( $z$ ) axis: **a–e** healthy and load condition. **f–j** Faulty and load condition



4.65%, respectively, whereas BSFC and FC were found to be increased by 10.19% and 5.59%, respectively, in faulty operating condition due to liner scuffing fault. This was due to the frictional losses in the piston–cylinder assembly caused by liner scuffing fault which allowed the combustion gasses to escape from the combustion chamber to the crankcase; this phenomenon is known as blow-by. These frictional losses caused the engine to consume more fuel for the required amount of power to be produced. The deficient mixture of air–fuel in the combustion chamber caused the engine to produce less power which result in poor thermal efficiency.

The exhaust emission parameters such as carbon monoxide (CO), carbon dioxide (CO<sub>2</sub>), hydrocarbon (HC), and nitrogen oxide (NO<sub>x</sub>) were measured using exhaust gas analyzer at distinct loading conditions and presented in Fig. 18a–d, respectively. It was clearly observed that due to liner scuffing fault, exhaust emissions parameters were increased significantly. An increment of 27.58%, 48.04%, 41.02%, and 43.89% in CO, CO<sub>2</sub>, HC, and NO<sub>x</sub> parameters were obtained due to liner scuffing fault, respectively. A liner scuffing fault caused blow-by losses in which some of the mixtures of air–fuel ratio from the combustion chamber escapes to the crankcase which resulted in the deficient mixture of air–fuel in the combustion chamber. The

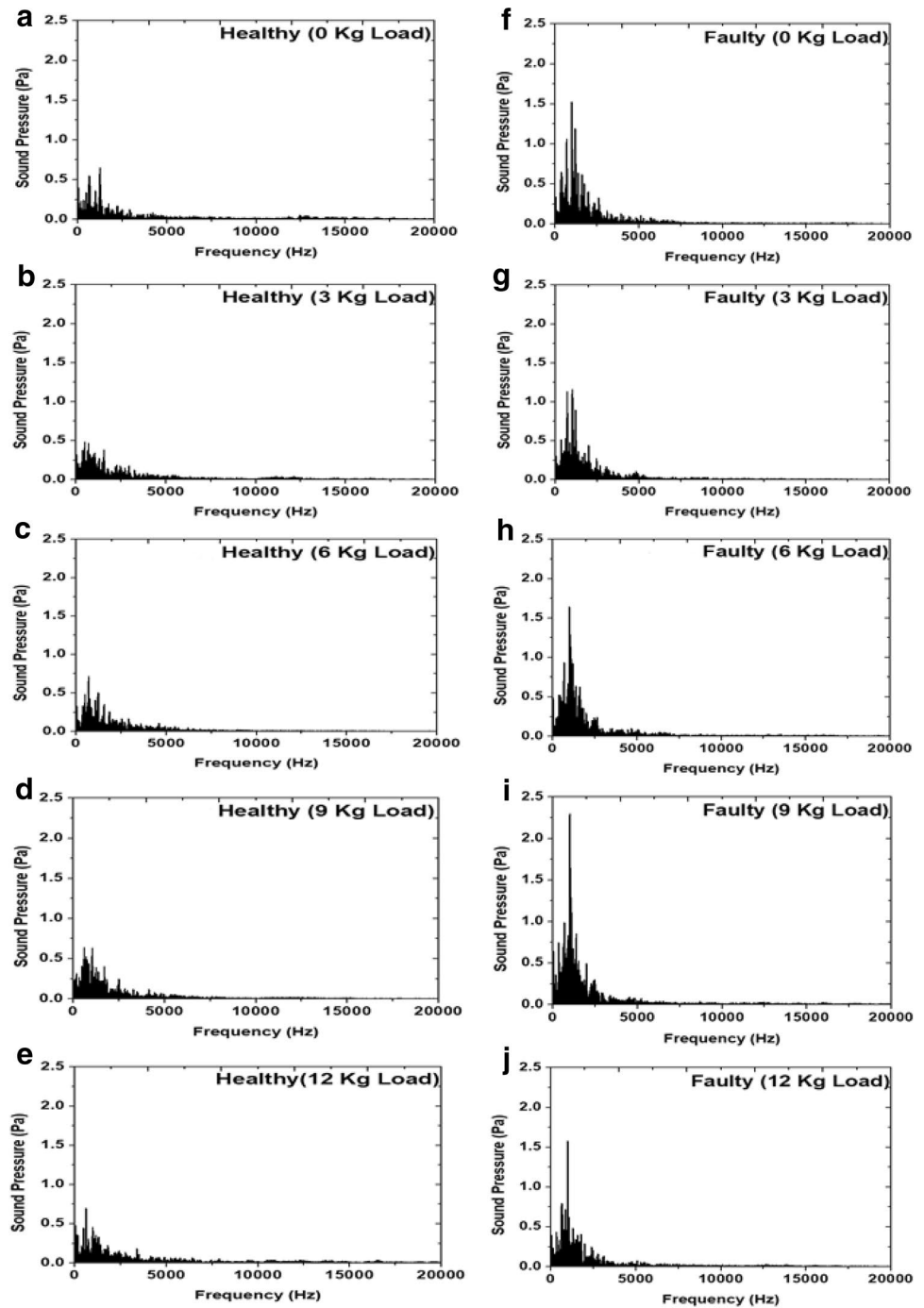
**Fig. 11** FFT spectra of engine vibrations in vertical (y) axis: **a–e** healthy and load condition. **f–j** Faulty and load condition



deficient mixture of the air–fuel ratio in the combustion chamber caused incomplete combustion. CO emission from the engine occurs due to the fuel-rich mixture as there was insufficient oxygen in the combustion chamber to convert all the carbon into carbon dioxide resulting in the increment of CO and CO<sub>2</sub> in the exhaust. The incomplete combustion results in unburned hydrocarbon which mixed with the combustion gasses and released to the atmosphere during the exhaust stroke. NO<sub>x</sub> emission from the engine was due to the deficient mixture of air–fuel ratio which caused incomplete combustion, thereby causing an increment in the exhaust.

The cylinder pressure inside the combustion chamber was monitored for both healthy and faulty operating conditions at various loads is depicted in Fig. 19a–e. It is clearly observed that the reduction in the cylinder pressure was obtained at all loading conditions. This was due to the liner scuffing fault which caused frictional and blow-by losses. The blow-by losses always increase in the worn out piston–cylinder assembly. As in this case, due to liner scuffing fault, most of the unburned air–fuel mixture and burned combustion gasses were escaped from the combustion chamber to the crankcase which affected the rate of pressure rise in the combustion chamber. The decrement in the combustion pressure

**Fig. 12** FFT spectra of acoustic signals under healthy and faulty operating conditions



affected engine brake power and brake thermal efficiency which was depicted clearly in Fig. 18a, b. During the power stroke, the uneven pressure was noticed at all the loading conditions.

## Summary and Conclusions

In the present research work, experimental investigations were carried out to detect the liner scuffing fault of a diesel engine using Fourier transform and statistical feature extracted from vibration and acoustic signals. Engine vibrations and acoustic signals were measured for both

**Fig. 13** Statistical features of engine vibration in longitudinal ( $x$ ) axis under healthy and faulty operating conditions

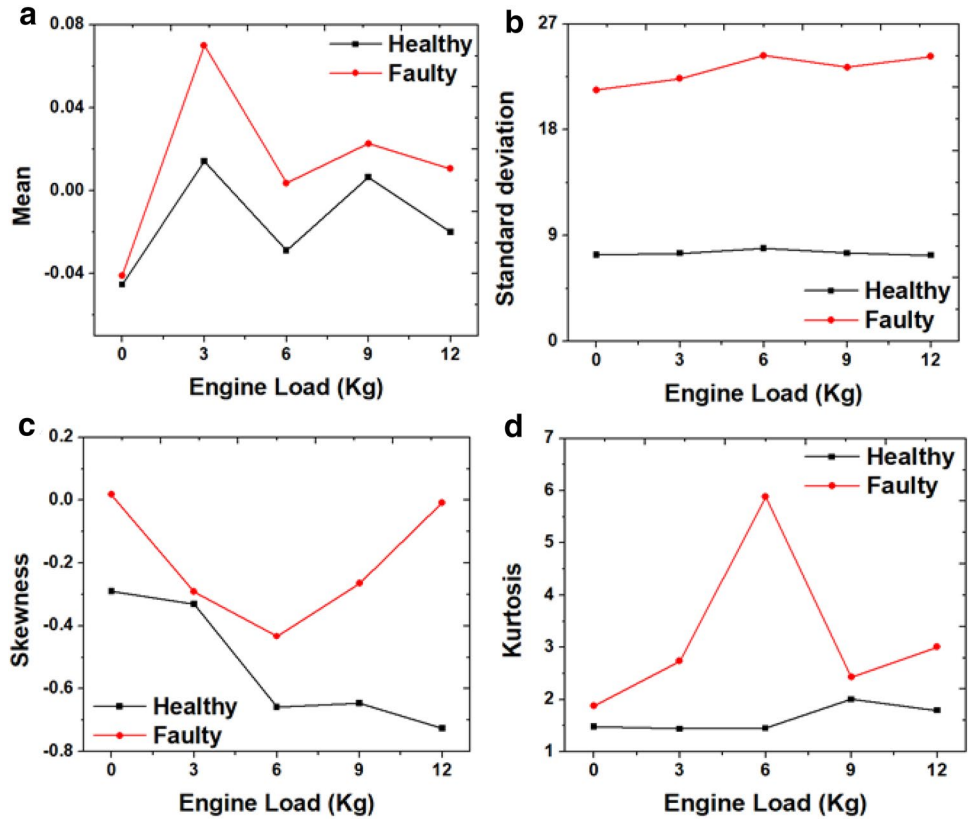


**Fig. 14** Statistical features of engine vibration in lateral ( $z$ ) axis under healthy and faulty operating conditions

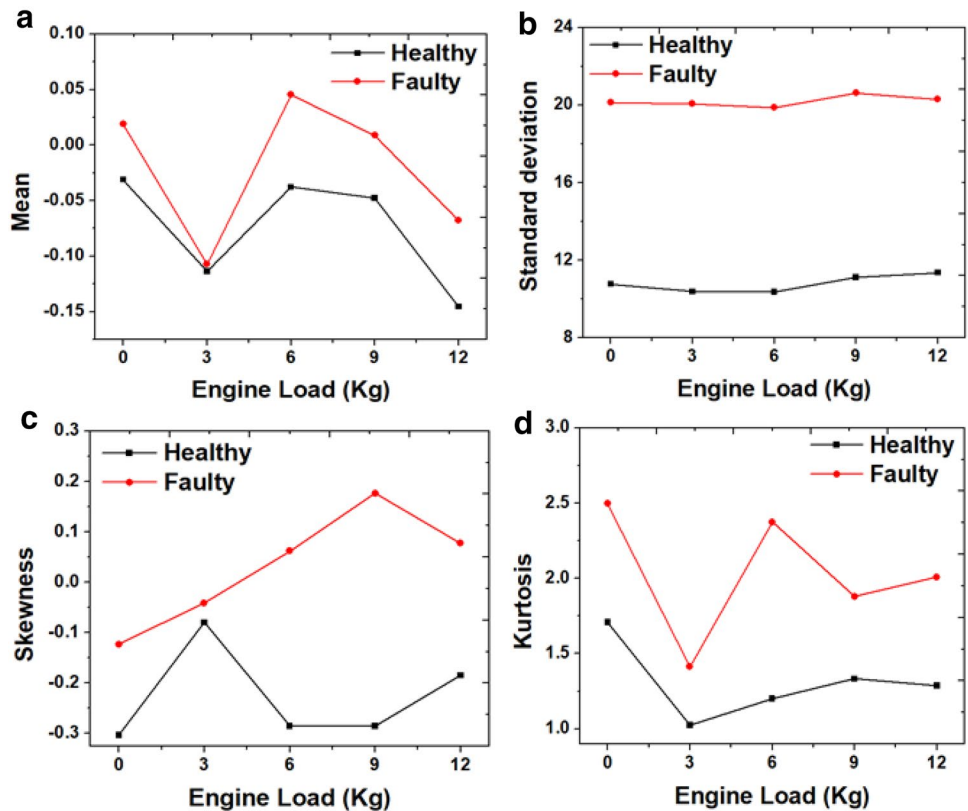


**Fig. 15** Statistical features of engine vibration in vertical (y) axis under healthy and faulty operating conditions

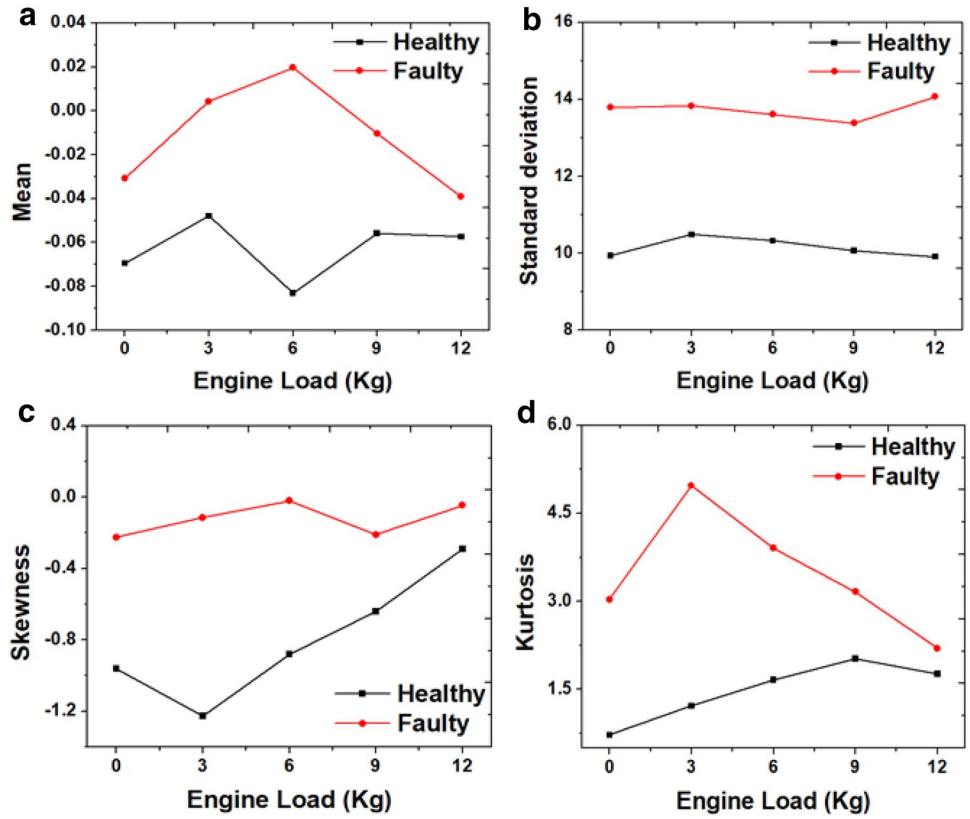


**Fig. 16** Statistical features of engine acoustic signals under healthy and faulty operating conditions

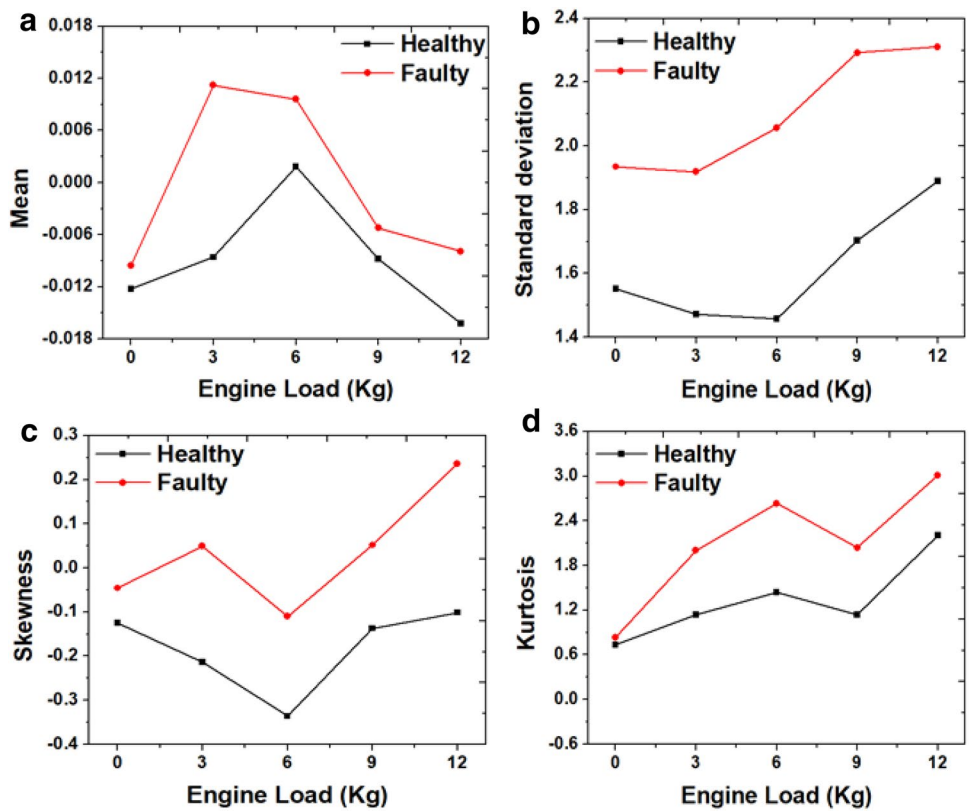




**Fig. 17** Performance parameters of the engine under healthy and faulty operating conditions: **a** BP, **b** BTh, **c** BSFC, and **d** FC

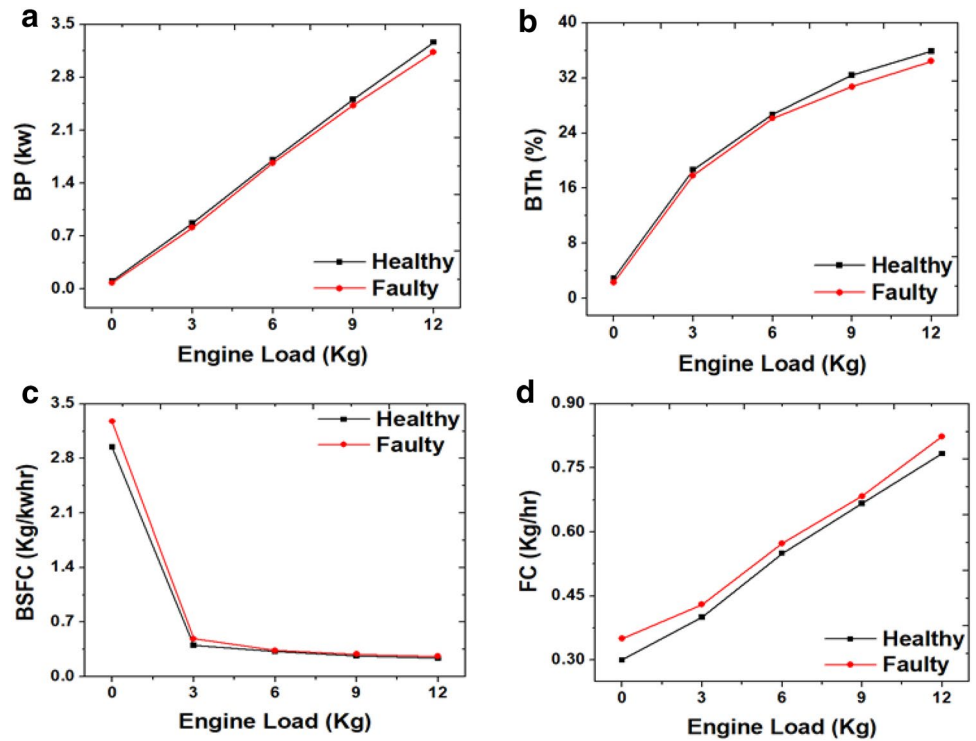
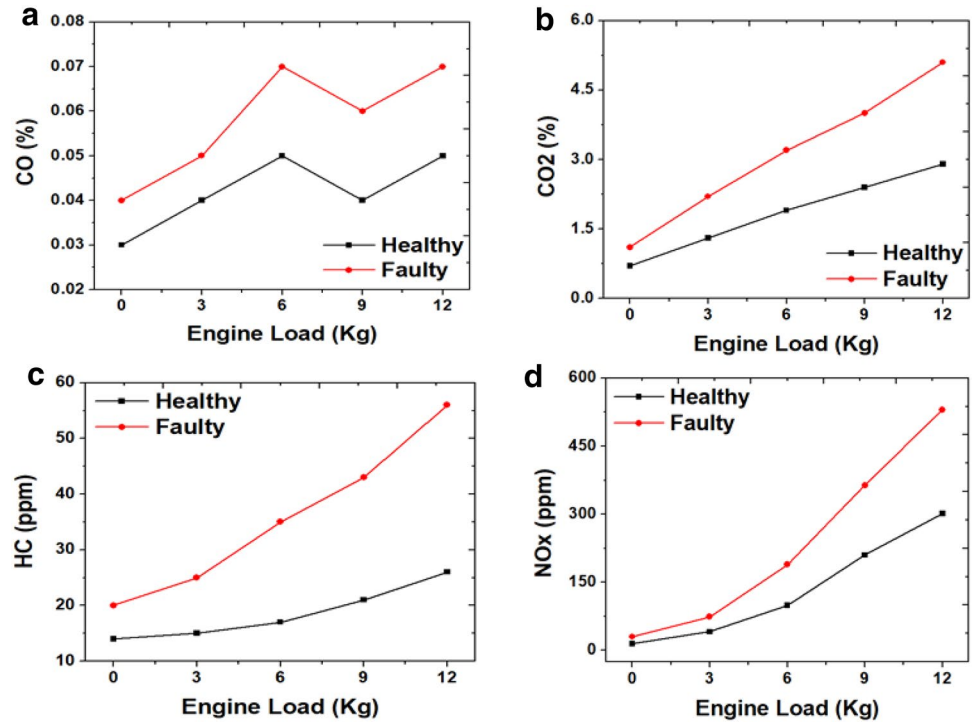


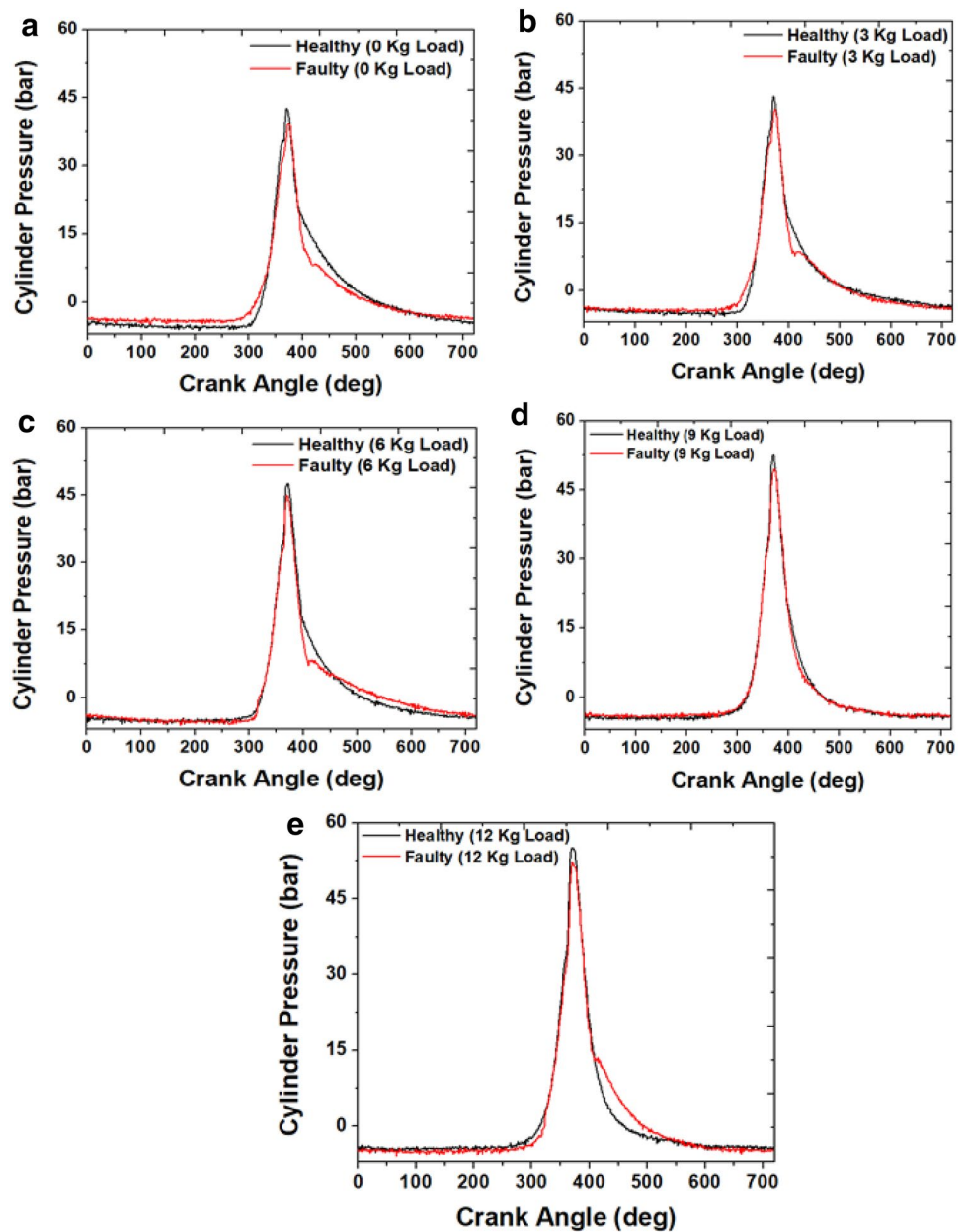
**Fig. 18** Emission parameters of the engine under healthy and faulty operating conditions: **a** CO, **b** CO<sub>2</sub>, **c** HC, and **d** NO<sub>x</sub>



healthy and faulty engine conditions. The performance and emission parameters were also analyzed in conjunction with vibration and acoustic signals. The following conclusions were drawn from the experimental investigations.

1. The higher amplitudes of vibrations were observed in all the axes at all the loading conditions due to liner scuffing fault. The maximum amplitudes of vibration were noticed at the longitudinal (*x*) and lateral (*z*) axes.

**Fig. 19** The variation of cylinder pressure under healthy and faulty operating conditions



- The sound pressure amplitudes were significantly affected by liner scuffing fault. The maximum sound pressure amplitude was perceived at 9 kg load.
- An increment in the statistical feature parameters of vibration and acoustic signals was perceived at all the loading conditions. The uneven trend of all the statistical feature parameters was due to the spurious effect of high-frequency amplitudes of vibration and acoustic signals.
- A significant decrement in BP and BTh by as much 4.10% and 4.65% and an increment in BSFC and FC by as much 10.19% and 5.59% were observed due to liner scuffing fault.
- An increment in the CO, CO<sub>2</sub>, HC, and NO<sub>x</sub> by as much 27.58%, 48.04%, 41.02%, and 43.89%, respectively, was observed due to liner scuffing fault.
- The cylinder pressure was significantly decreased at all the loading conditions due to frictional and blow-by losses caused due to liner scuffing fault.

It is postulated that the aforementioned methods can be employed in the fault detection analysis of engine components, particularly for liner scuffing fault. Early detection of the liner scuffing fault can avoid other component failures, system shut down, and catastrophic failure involving human fatalities and economic losses.

## References

- Liu Z, Wu K, Ding Q, Gu JX (2019) Engine misfire diagnosis based on the torsional vibration of the flexible coupling in a diesel generator set: simulation and experiment. *J Vib Eng Technol*. <https://doi.org/10.1007/s42417-019-00097-1>
- Merkisz-Guranowska A, Waligórski M (2018) Recognition and separation technique of fault sources in off-road diesel engine based on vibroacoustic signal. *J Vib Eng Technol* 6(4):263–271
- Moosavian A, Najafi G, Ghobadian B, Mirsalim M, Jafari SM, Sharghi P (2016) Piston scuffing fault and its identification in an IC engine by vibration analysis. *Appl Acoust* 102:40–48
- Moosavian A, Najafi G, Ghobadian B, Mirsalim M (2017) The effect of piston scratching fault on the vibration behavior of an IC engine. *Appl Acoust* 126:91–100
- Chiatti G, Chiavola O, Palmieri F (2017) Vibration and acoustic characteristics of a city-car engine fueled with biodiesel blends. *Appl Energy* 185:664–670
- Gutierrez M, Castillo A, Iniguez J, Reyes G (2017) Measurement of engine vibrations with a fuel blend of recycled lubricating oil and diesel oil. In: SAE technical paper. <https://doi.org/10.4271/2017-01-2333>
- Barelli L, Bidini G, Buratti C, Mariani R (2009) Diagnosis of internal combustion engine through vibration and acoustic pressure non-intrusive measurements. *Appl Therm Eng* 29(8–9):1707–1713
- Çelebi K, Uludamar E, Özcanlı M (2017) Evaluation of fuel consumption and vibration characteristic of a compression ignition engine fuelled with high viscosity biodiesel and hydrogen addition. *Int J Hydrogen Energy* 42(36):23379–23388
- Uludamar E, Yıldızhan Ş, Aydın K, Özcanlı M (2016) Vibration, noise and exhaust emissions analyses of an unmodified compression ignition engine fuelled with low sulphur diesel and biodiesel blends with hydrogen addition. *Int J Hydrogen Energy* 41(26):11481–11490
- Taghizadeh-Alisaraei A, Ghobadian B, Tavakoli-Hashjin T, Mohtasebi SS, Rezaei-asl A, Azadbakht M (2016) Characterization of engine's combustion-vibration using diesel and biodiesel fuel blends by time-frequency methods: a case study. *Renew Energy* 95:422–432
- Çelebi K, Uludamar E, Tosun E, Yıldızhan Ş, Aydın K, Özcanlı M (2017) Experimental and artificial neural network approach of noise and vibration characteristic of an unmodified diesel engine fuelled with conventional diesel, and biodiesel blends with natural gas addition. *Fuel* 197:159–173
- Uludamar E, Tosun E, Aydın K (2016) Experimental and regression analysis of noise and vibration of a compression ignition engine fuelled with various biodiesels. *Fuel* 177:326–333
- Taghizadeh-Alisaraei A, Ghobadian B, Tavakoli-Hashjin T, Mohtasebi SS (2012) Vibration analysis of a diesel engine using biodiesel and petrodiesel fuel blends. *Fuel* 102:414–422
- Taghizadeh-Alisaraei A, Rezaei-Asl A (2016) The effect of added ethanol to diesel fuel on performance, vibration, combustion and knocking of a CI engine. *Fuel* 185:718–733
- Jena DP, Panigrahi SN (2014) Motor bike piston-bore fault identification from engine noise signature analysis. *Appl Acoust* 76:35–47
- Chiatti G, Chiavola O, Palmieri F, Piolo A (2015) Diagnostic methodology for internal combustion diesel engines via noise radiation. *Energy Convers Manag* 89:34–42
- Jenkins SH (1975) Analysis and treatment of diesel-engine noise. *J Sound Vib* 43(2):293–304
- JunHong Z, Bing H (2005) Analysis of engine front noise using sound intensity techniques. *Mech Syst Signal Process* 19(1):213–221

**Publisher's Note** Springer Nature remains neutral with regard to jurisdictional claims in published maps and institutional affiliations.